metals

MDPI

Article

Very High Cycle Fatigue Behavior of Austenitic Stainless Steels with Different Surface Morphologies

Marek Smaga *, Annika Boemke, Dietmar Eifler and Tilmann Beck

Institute of Materials Science and Engineering, TU Kaiserslautern, 67663 Kaiserslautern, Germany
* Correspondence: smaga@mv.uni-kl.de; Tel.: +49-631-205-2762

Abstract: The fatigue behavior of the two austenitic stainless steels AISI 904L and AISI 347 with different surface morphologies, (i) conventionally turned and finally polished, (ii) cryogenic turned using CO_2 snow, as well as (iii) cryogenic turned and finally polished, was investigated using an ultrasonic fatigue testing system up to the very high cycle fatigue regime using an ultrasonic fatigue testing system. The AISI 904L is stable against deformation-induced phase formation while the AISI 347 is in the metastable state and shows martensite formation induced by cryogenic turning as well as mechanical loading. For the detailed characterization of the surface morphology, confocal microscopy, scanning electron microscopy, and X-ray diffraction methods were used. The specimens from stable austenite failed in the high cycle fatigue and very high cycle fatigue regime. Opposed to this, the metastable austenite achieved true fatigue limits up to load cycle $N = 1 \times 10^9$ and failed only in the high cycle fatigue regime. Furthermore, due to surface modification, an increase of fatigue strength of metastable AISI 347 was observed.

Keywords: austenitic stainless steels; metastability; surface morphology; VHCF

Citation: Smaga, M.; Boemke, A.; Eifler, D.; Beck, T. Very High Cycle Fatigue Behavior of Austenitic Stainless Steels with Different Surface Morphologies. *Metals* **2022**, *12*, 1877. https://doi.org/10.3390/met12111877

Academic Editor: Martin Heilmaier

Received: 30 September 2022
Accepted: 31 October 2022
Published: 3 November 2022

1. Introduction

It is well known that austenitic stainless steels (ASSs) can exist in stable or metastable state dependent on their chemical composition [1,2]. Hence, the paramagnetic austenite can transform due to plastic deformation to a more stable microstructure, i.e., paramagnetic ε-martenisite and/or ferromagnetic α'-martensite [3]. Because during the discovery of ASSs the passivity (and hence "stainlessness") was the main scope of material development and not the metastability as well as its influence on the mechanical and physical behavior, still extensive experimental work is done at this class of materials. Investigations of ASSs up to the very high cycle fatigue (VHCF) regime show different fatigue behavior depending on their level of metastability. Carstensen et al. [4] performed fatigue tests with tubes of stable AISI 904L and determined specimen failure in the VHCF regime with crack initiation at the surface. Therefore, in stable austenitic stainless steels, no classical fatigue limits up to load cycles $N = 10^7$ exist. Comparable results for AISI 316L were found by Lago et al. [5]. A continuous decrease of fatigue strength was detected up to $N = 1 \times 10^9$. Crack initiation occurred at the surface at all specimens. Subsurface fish-eye fracture without inclusion in austenitic stainless steel SUS 316NG was observed in pre-strained specimen by Takahashi et al. [6] as well as surface crack initiation in the VHCF regime. Grigorescu et al. [7,8] investigated additionally to "quasi-stable" AISI 316L the metastable austenitic AISI 304L. For AISI 304L, a true fatigue limit was detected associated with α'-martensite formation, i.e., specimen failure of AISI 304L only occurs below $N = 1 \times 10^6$ load cycles. For AISI 904L, a clear decrease of fatigue strength in VHCF regime occurs with crack initiation at twin boundaries [7].

Since specimen failure in VHCF regime of ASSs occurred only in the case of the stable austenite and crack initiation occurs mostly on the surface [4,5], surface modification seems to be one possibility to increase the fatigue strength, even in the VHCF regime. The

modification of surface morphology improves for stable and metastable ASSs the fatigue strength in the low cycle (LCF) and in the high cycle regime (HCF). Consequently, numbers of cycle higher than $N > 10^7$ can be applied at relatively high stress amplitudes without specimen failure. Hence, the crack initiation and fatigue process of ASSs with modified surface morphologies must be characterized. In the literature, different methods were used for surface modification of austenite, e.g., ultrasonic surface modification [9], cryogenic deep rolling [10], or cryogenic turning [11,12]. All these methods lead to an increase of fatigue strength in LCF and/or HCF regime due to the resulting nanostructured layers and, in the case of the metastable ASSs, ε and/or α´-martensite formation [13,14]. Up to now, only few results of fatigue life in VHCF regime for specimens with modified surface from ASSs exist [15]. Therefore, the research presented in this paper focused on the VHCF behavior of austenitic stainless steels with different surface morphologies. Both type ASS, stable AISI 904L and metastable AISI 347, were investigated. The surface modification was produced by cryogenic turning [11,12]. The fatigue tests were performed with an ultrasonic testing system, developed at the authors' institute [16].

2. Materials and Methods

2.1. Austenitic Stainless Steels

The investigated materials were the stable austenitic steel AISI 904L in solution annealed state (T = 1100 °C, t = 30 min, quenched in H_2O) and the metastable austenitic stainless steel AISI 347, also solution annealed (T = 1050 °C, t = 35 min, quenched in He). Both materials consist of a purely austenitic microstructure in the initial state, have no preferred crystallographic orientation, and contain twins from solution annealing (Figure 1). The grain size including twins is 38 µm for the AISI 904L and 17 µm for the AISI 347. Optical micrographs (Figure 1b,d) show, aside from the grain structure, a band-like structure in the axial direction of the specimen, which indicates a heterogeneity in the chemical distribution [17]. To characterize the metastability of both materials, the $M_{s,Eichelmann}$ temperature [18], $M_{d30,Angel}$ temperature [19], and stacking fault energy (SFE) [20] were calculated according to the chemical composition of the investigated materials (Table 1). The values indicate the stability of AISI 904L and the metastability of AISI 347. Consequently, the metastable AISI 347 is prone to deformation-induced transformation from paramagnetic γ-austenite to paramagnetic ε-martensite as well as to ferromagnetic α´-martensite. Mechanical properties determined in tensile tests at ambient temperature estimated according to the DIN 50125 standard as well as ferromagnetic α´-martensite fractions after specimen failure measured by magnetic Feritscope™ signal (ξ) in FE-% [2] are given in Table 2.

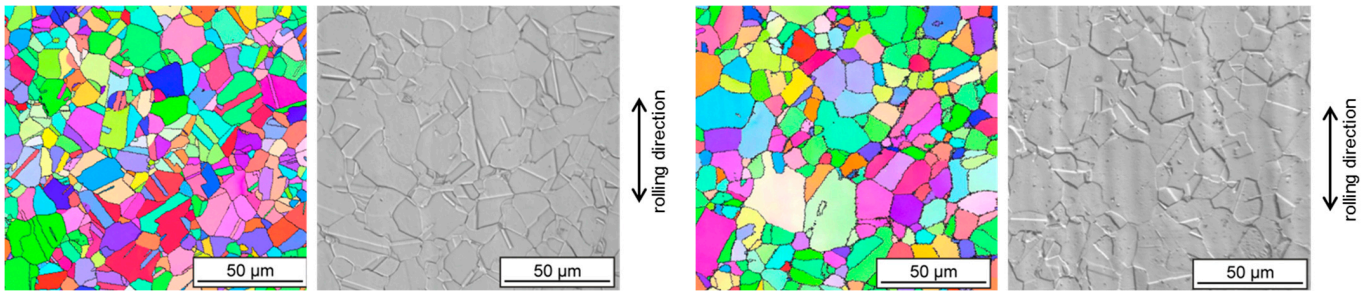

Figure 1. Initial microstructure of (**a**) stable AISI 904L and (**b**) metastable AISI 347. EBSD maps with grain orientation and optical micrographs after V2A etching.

Table 1. Chemical composition of the investigated austenitic stainless steel in wt%.

	C	N	Cr	Ni	Nb	Mo	Cu	Mn
AISI 904L (stable)	0.03	0.06	19.92	24.34	0.03	4.22	1.42	0.95
AISI 347 (metastable)	0.02	0.02	17.19	9.44	0.39	0.23	0.11	1.55

Table 2. Mechanical properties, austenite stability parameters, and α'-martensite fraction (ξ) after specimen failure in tensile tests.

	Young's modulus in GPa	$R_{p0.2}$ in MPa	UTS in MPa	$M_{d30,Angel}$ in °C	$M_{s,Eichelmann}$ in °C	SFE in mJ/m^2	ξ in FE-%
AISI 904L (stable)	187	307	631	−220	−1156	54	0
AISI 347 (metastable)	179	225	603	46	-87	26	15

2.2. Experimental Methods

An ultrasonic fatigue testing (USFT) system built at the authors' institute was used for the fatigue tests. The working frequency was ~20 kHz, which was generated by an ultrasonic generator and transformed in a mechanical oscillation by a converter. The specimen was fixed on one hand at a booster which was attached at the converter that amplified the oscillation about factor 2.5. The displacement amplitude at the bottom end of the specimen was measured by a laser vibrometer CLV-2534 from Polytec. The oscillation signal was recorded with a sample rate of 500 kHz. With this experimental setup, the fatigue tests were continuously monitored, and the exact number of cycles could be determined. To perform reliable fatigue tests with the USFT system, an exact pulse shape with short onset and decay times as well as a stable stationary phase must be achieved, a constant displacement stress amplitude must be ensured throughout the complete test, and as the pulse-pause ratio needs to be selected in such a way that excessive specimen heating due to the high-frequency loading is avoided [21]. The temperature in the specimen gauge length was measured by an IR-pyrometer. The temperature change ΔT_{Pulse} is defined as the difference of the measured absolute temperature at the beginning and the end of the pulse. The maximum temperature of the specimen during the tests was limited to 50 °C. The specimens were additionally cooled with compressed air (Figure 2a).

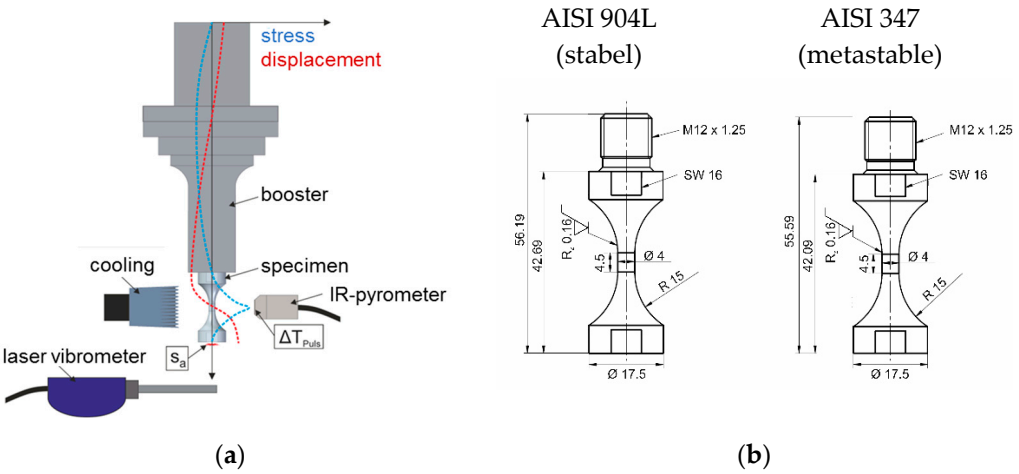

Figure 2. Schematic view of the operating principle of the ultrasonic fatigue testing system with the development of displacement and stress, as well as in situ measurements during the tests (**a**) and specimen geometry (**b**).

The geometry of the specimens is given in Figure 2b. The maximum stress amplitude was calculated based on steady state FEM simulations in ABAQUS assuming a linear

relationship between the stress amplitude (σ_a) and the displacement amplitude (s_a) at the lower end of the specimen measured by a 1-axis laser vibrometer. A linear correlation factor k between stress amplitude and displacement amplitude of k_{904L} = 23.6 MPa/µm for AISI 904L and k_{347} = 22.7 MPa/µm for AISI 347 was determined. Accordingly, only the stress amplitude is used to describe the fatigue results. Due to the highly transient material behavior of metastable ASSs, the ultrasonic fatigue testing is very challenging. Already a small increase of the α'-martensitic phase leads to a pronounced change of the displacement amplitude as well as the pulse shape. Consequently, to perform VHCF tests on metastable austenite from N = 0 up to the limiting number of cycles, e.g., $N_l = 1 \times 10^9$ at the USFT stystem, a continuous adjustment of the control parameters must be performed, as described in [22].

To characterize the microstructure, metallographic preparation of the sections was performed by grinding up to 1200 grit and electronical polishing. For optical micrographs metallographic sections were etched using V2A solution. The optical micrographs were obtained using a Leica DM 6000 M. Detailed analyses of the crystallographic microstructure were carried out using an SEM/FIB GAIA3 (Tescan s.r.o., Brno, Czech Republic) equipped with an EBSD module "Hikari Plus". The inverse pole figure maps were generated in the normal direction using OIMA software. X-ray diffraction phase analysis was performed using a Bragg Brentano configuration on a PANalytical X'Pert PRO MRD X-ray diffractometer using $CuK_{\alpha 1}$ radiation. The diffractograms were acquired over a range of 2θ = 40° to 100° using a step-size of 0.04°. Phase analyses were performed by using the Rietveld method. To minimize the influence of texture, the diffraction profiles were measured at five different tilt angles in the range 0–40° with relative errors in the quantification of the phase contents of about 1–3% for each phase. The same setup was used to perform residual stress measurements on the surface at all considered ablation depths. In this context, all measurements focusing on the (022) γ-austenite plane were measured from χ = −45° to +45° tilt angle at a step size of 8.2°. The type I residual stresses determined with the $\sin^2\psi$ method were measured in axial direction. The maximum measurement spot size on the specimen surface used for the phase analyses and the residual stress measurements were, with approx. 1.5 mm × 1.5 mm, significantly smaller than the material areas removed for depth-resolved investigation of the specimen surface layer. These areas were removed by electrolytic ablation using a Struers LectroPol-5 from the specimen surface to a depth of 400 µm between the XRD measurements. The temperature of the cooled electrolyte remained permanently below 20 °C during the ablation process to avoid microstructural changes. Furthermore, an ablation strategy with local removal was applied which, in contrast to a full-surface removal of material layers, has a way smaller influence on the overall residual stresses [23]. The magnetic Feritscope™ measurements were used for detailed characterization of deformation-induced α'-martensite formation. The Feritscope™ magnetic fraction (ξ) is given in volume percent ferrite (FE-%), without converting into α'-martensite content. In literature, a linear correlation between FE-% and α'-martensite content is reported [24].

3. Results

3.1. Surface Morphology

As mentioned above, specimens with different surface morphologies were investigated. Two different manufacturing processes were used for surface modification: conventional turning and cryogenic turning. Specimens from both materials were polished after conventional turning, such that the fatigue behavior could be analyzed in a reference state. These specimens consisting of purely austenitic microstructure in the volume as well as in the near surface area have a smooth surface in the gauge length. The surface morphologies produced by conventional turning and subsequently polishing are called SSL_p (Stable Surface Layer polished) for AISI 904L and ASL_p (Austenitic Surface Layer polished) for AISI 347. The second production process was a cryogenic turning at the Institute for Manufacturing Technology and Production Systems, TU Kaiserslautern, Germany. The specimens were

cooled with CO_2 snow using two attached nozzles at the CNC lathe. The chosen cutting speed was v_c = 30 m/min, the depth of cut a_p = 0.2 mm and the two feeds f_1 = 0.15 and f_2 = 0.35 mm/rev (Table 3). More details about the cryogenic turning process were published elsewhere, see e.g., [11,12].

Table 3. Investigated surface morphologies.

AISI 904L	Stable Surface Layer polished	SSL_p
	Stable Surface Layer turned with f = 0.15 mm/rev	SSL_{t015}
	Stable Surface Layer turned with f = 0.35 mm/rev	SSL_{t035}
AISI 347	Austenitic Surface Layer polished	ASL_p
	Martensitic Surface Layer polished	MSL_p
	Martensitic Surface Layer turned with f = 0.15 mm/rev	MSL_{t015}
	Martensitic Surface Layer turned with f = 0.35 mm/rev	MSL_{t035}
	Martensitic Surface Layer of pre-deformed and finial turned with f = 0.35 mm/rev	MSL_{dt035}

To eliminate the relatively high roughness formed by the turning process and to investigate only the influence of the martensitic surface layer on the fatigue behavior, the specimens of the metastable AISI 347 were manufactured by cryogenic turning with lower feed f_1 = 0.15 mm/rev and subsequently polished. This morphology is named MSL_p for Martensitic Surface Layer polished. The mean roughness (R_z) of the surfaces of all investigated morphologies determined with confocal microscopy is given in Figure 3. In general, three levels of the roughness in dependency of the feed rate can be seen (Figure 3a). The polished specimens have a smooth surface with an average roughness value below R_z = 1 µm. The roughness values of the turned specimen is dominated by the grooves resulting from the chosen feed in turning process. Hence, the low feed rate f_1 = 0.15 mm/rev leads to smaller R_z of ~4 µm and higher f_2 = 0.35 mm/rev to higher R_z up to ~11 µm, while the polished surface is standard for fatigue tests, which focus on the determination of fatigue limits of the materials, the turned variants represent typical technical surfaces. Generally, the surface roughness has a large influence of the fatigue properties and typically reduces fatigue life. However, previous results for metastable austenitic steles show that the negative influences of the high surface roughness of fatigue life in the LCF/HCF regime can be compensated by near surface martensite formation during cryogenic turning [11,12], which opens a new perspective to increase the fatigue life of components.

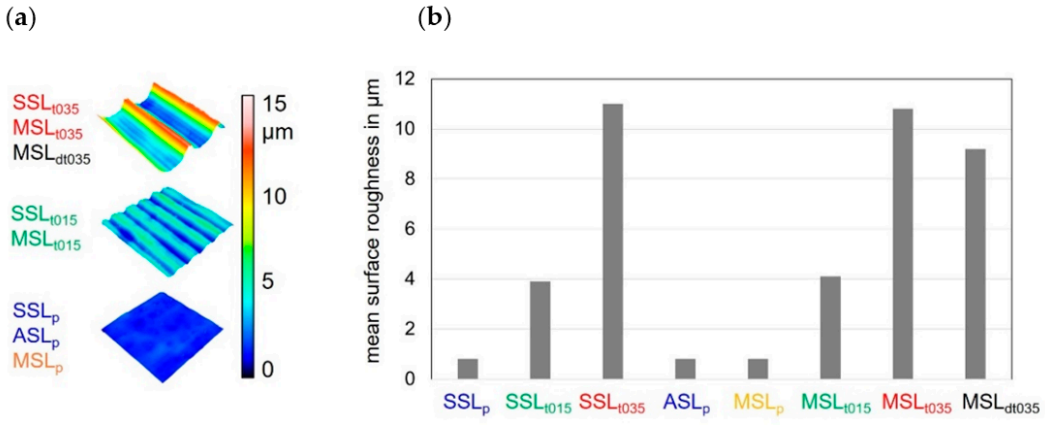

Figure 3. Confocal microscopy images of three representative surface topographies after cryogenic turning with f = 0.35 mm/rev, 0.15 mm/rev, and electrolytical polishing (**a**) as well as the mean surface roughness R_z for all morphologies (**b**).

Scanning-ion microscopy (SIM) investigations were performed at FIB cross sections, which were positioned in the gauge length of the VHCF specimens in axial direction in the

middle of a turning groove (Figure 4). ASL_p and SSL_p show the microstructure as the initial state (comp. Figure 1), i.e., purely austenitic grains with different grain size. No influence of the production process can be observed. In contrast to that, the cryogenic turned specimens show a nanocrystalline layer (NL) under the surface, with a maximum layer thickness of about 5 µm caused by cryogenic turning. A dependency of the NL thickness on the feed rate cannot be seen. SIM micrographs of the MSL_{dt035} sample indicated aside from the NL a fine microstructure, which is a result of pre-deformation before final cryogenic turning.

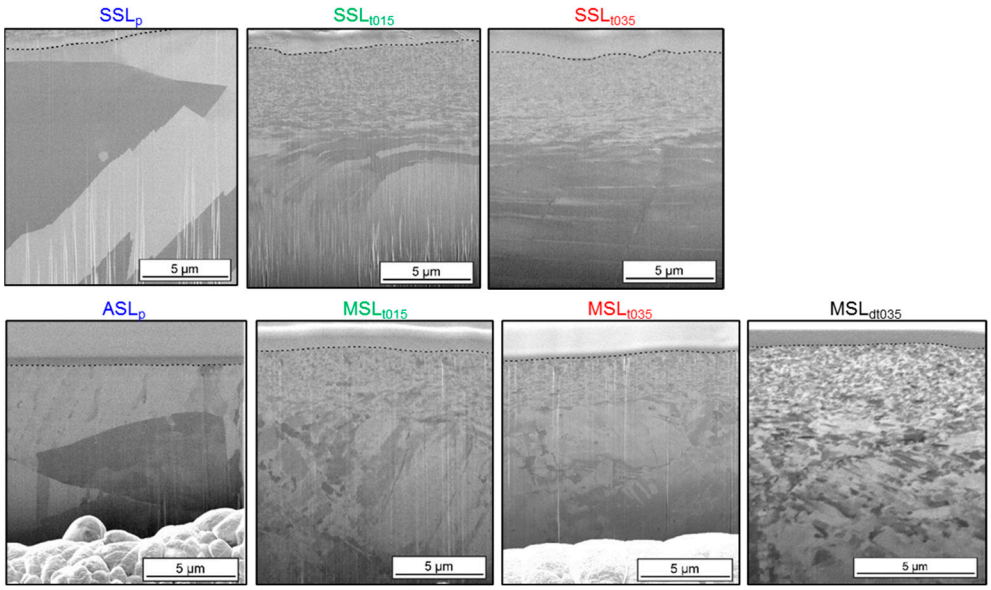

Figure 4. Scanning-ion microscopy images of the near surface microstructure of the investigated morphologies.

Aside from the surface roughness (Figure 3) and near surface microstructure (Figure 4), residual stresses and phase distribution below the specimens' surface influence the fatigue performance. Figure 5 shows the residual stresses (σ_{RS}) and phase distributions of all investigated morphologies. The information for polished specimens (SSL_p, ASL_p, MSL_p) correspond to the state at a distance of about 20–30 µm from the surface. All morphologies show relatively high tensile σ_{RS} at the specimen surface. The maximum σ_{RS} = 750 MPa was measured at MSL_{dt035} and the smallest one on MSL_{t015} with σ_{RS} = 400 MPa. The σ_{RS} reduced to nearly zero at ~50 µm distance from the surface for MSL_{t015} specimens. The residual stresses for MSL_{d035} decreased from σ_{RS} = 750 MPa to 200 MPa at ~100 µm distance from the surface and remained constant. A typical change from tensile to compressive residual stress as described in literature [25] was only observed for MSL_{t035}. Note that, since the specimens with the morphologies ASL_p, SSL_p, SSL_{t015}, and SSL_{t035} consist of a purely austenitic microstructure, the respective phase distributions are not shown in Figure 5. Γ-austenite, α'- and ε-martensite content was measured in the other morphologies of AISI 347 (MSL_{t015}, MSL_{t035}, and MSL_{dt035}). All three morphologies have a maximum content of α'-martensite not directly at the surface but in some distance from the surface: MSL_{t015} at 15 µm with α' = 18 vol.%, MSL_{t035} at 80 µm with α' = 23 vol.% and MSL_{dt035} at 12 µm with 45 vol.%, which corresponds to the fraction caused by pre-deformation. The penetration depth of the X-ray is a few micrometers, so in the first X-ray step, the nanocrystalline structure strongly influences the measurement. However, the strong decrease of α'-martensite in the MSL_{dt035} from 45 vol.% to 23 vol.% indicates a possible back transformation to austenite during the manufacturing process. Only minimal amounts of ε-martensite were found. The MSL_{t015} shows a slightly lower α'-martensite content, which at 98 µm drops to almost 0 vol.%. This coincides with findings in the literature, which show higher α'-martensite proportions with increasing feed in the cryogenic turning [12]. With the disappearance of α'-martensite, small proportions ε-martensite appear of maximum 7 vol.%.

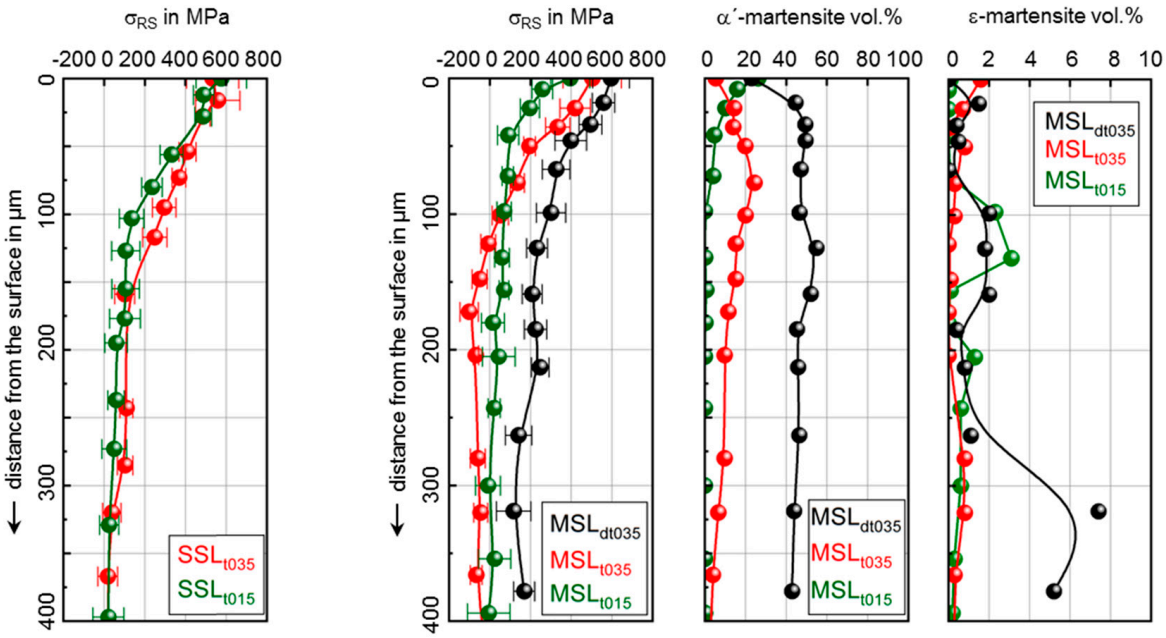

Figure 5. Distribution of residual stresses and phases content until the specimen surface.

3.2. Fatigue Behavior of Stable AISI 904L with Different Surface Morphologies

To study the fatigue behavior of the stable ASS, single step fatigue tests at a load ratio R = −1 were realized at room temperature up to the VHCF range with a maximum number of load cycles of 1×10^9 with the ultrasonic fatigue system with the load frequency of ~20 kHz (see Section 2.2). The S-N diagram of the samples with the three different surface morphologies is shown in Figure 6; run out is marked with an arrow. The specimens with the morphology SSL_p failed in the HCF and the VHCF regime. With decreasing stress amplitude, the number of cycles to failure increased until the ultimate number of cycles is reached. Hence, no classical fatigue limit exits. A similar fatigue behavior was also observed by Carstensen et al. in fatigue tests at thin tubular specimens from AISI 904L [4]. At a stress amplitude of σ_a = 306 MPa, the tested sample with SSL_p reaches the limiting number of cycles without failure. All cryogenically turned specimens exhibit earlier failures than the specimens with SSL_p at the same stress amplitude, where the sample with the morphology SSL_{t015} had the lowest lifetime. Specimen failure occurred only at the specimens' surface due to the high roughness of R_z = 4 µm (SSL_{t015}) and R_z = 11 µm (SSL_{t035}) in HCF regime. The influence of the surface roughness and the high tensile residual stresses seem to be predominant compared to the positive influence of the nanocrystalline structure (Figure 4), which in general reduces the plastic deformation in the specimen [13]. Therefore, no increase of fatigue life was achieved by cryogenic turning of stable ASS. Feritescope™ measurements confirm that no phase transformation occurred during the fatigue tests. Fractographic investigations on the failed specimens with SSL_p show that for $N_f > 1 \times 10^8$, the crack initiation changes from the surface to the volume (Figure 6). Volume defects, such as inclusions, could not be detected. Note that internal cracks can also occur in metallic materials without the presence of inclusions and, e.g., stress concentrations at the grain boundaries can have a crack-initiating effect, especially in the VHCF regime [26,27]. Takahashi and Ogawa also detected on a prestressed sample in compression an internal crack with a fish-eye structure without any internal defect [6]. However, in most cases when examining ASSs up to the VHCF range, surface cracks or cracks originating in the immediate vicinity of the surface are observed [4,5,28]. Bright areas are visible around the start of the crack at a distance of a few 100 µm on which there are extrusions (Figure 6). Probably during micro-crack growth, two halves of the sample do not have contact with each other and in this area, the extrusions developed at the surface fracture.

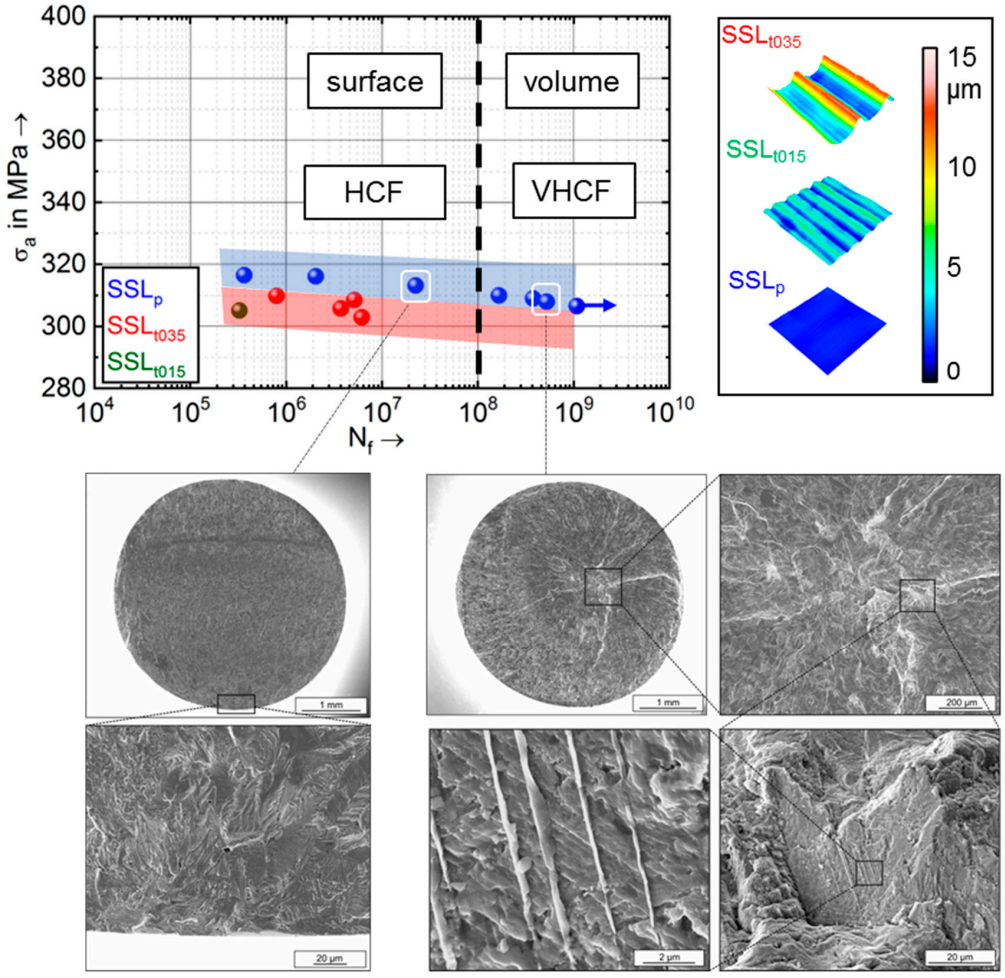

Figure 6. S-N diagram of AISI 904L with different surface morphologies and investigation of the fracture surface, run outs are marked with an arrow.

3.3. Fatigue Behavior of Metastable AISI 347 with Different Surface Morphologies

The influence of metastability on the VHCF behavior is very clearly seen by comparison of the S-N curves of both ASSs (Figures 6 and 7); run outs are marked with an arrow. The specimens from metastable AISI 347 with purely austenitic microstructure in the initial state and with different surface morphology only failed in the HCF regime at $N < 10^7$. In the VHCF regime, no specimen failure occurred, which shows that a true fatigue limit exists for this metastable austenite. Only the pre-deformed specimens failed in the VHCF regime, which is consistent with literature for different metastable austenitic steels [8,29,30]. During cyclic loading, the metastable AISI 347 transforms from paramagnetic γ-austenite to ferromagnetic α'-martensite, which is confirmed by Feritscope™ measurements. Hence, the surface morphology influences the fatigue behavior of metastable AISI 347 completely differently in comparison to the stable AISI 904L. The specimens with morphology MSL_{t035}, which exhibit nanocrystalline and martensitic layers show higher fatigue strength despite of the higher roughness values (R_z = 11 µm) and tensile residual stresses (504 MPa) than the conventionally turned and polished specimens with the ASL_p morphology and resulting small roughness of R_z = 1 µm and compressive residual stresses (−20 MPa). The fatigue strength of specimens increased after cryogenic turning about 50 MPa. The scatter of MSL_{t035} specimens failed in the HCF-regime was higher than that of the variant ASL_p, which is caused by the turning process resulting in irregularities by chip formation and chip breaking. The results show that the martensitic surface layer in combination with the nanocrystalline structure had a very positive effect on the fatigue behavior in VHCF regime, whereas only a nanocrystalline structure did not lead to higher fatigue life as shown for

stable AISI 904L (comp. fatigue life SSl_p with SSL_{t035} in Figure 6). This results from the low roughness, the martensitic surface layer, and the compressive residual stresses at the specimens' surface. The fatigue tests with MSL_{dt035} specimens were demanding the maximum displacement amplitude of the ultrasonic using testing system. It was not possible to perform higher stress amplitudes than σ_a = 381 MPa due to the high internal friction of the austenite in the specimens' volume. Nevertheless, an increase of fatigue strength for the morphology MSL_{dp} was determined. In contrast to the results from specimens without pre-deformation, failure in the VHCF regime occurred in specimens with the morphology MSL_{dt035} and the data points show a drop in the S-N diagram. Such behavior could also be observed in a metastable austenite with a α'-martensite content of 54 vol.% achieved by pre-deformation [30]. Using scanning electron micrographs, the fracture surfaces of specimens with the morphology MSL_{dt035} were examined. Figure 7 shows SEM micrographs of the MSL_{dp} specimen failed at N = 2.8 × 10^8 cycles. The fracture surface contains an AlCaO inclusion, and a niobium carbide a few microns below the surface. The fracture topography around the NbC indicates that crack initiation originated from the carbide. Hence, the deeper located subsurface AlCaO inclusion was fractured by crack growth. In general, the pre-deformation with deformation-induced martensite formation increases the HCF fatigue strength. However, in the VHCF regime, a drop of fatigue strength occurred. Taking into account the fatigue life of the specimen with the morphology MSL_p, it becomes clear that, even compared to the cryogenically turned samples with partially converted volume (morphology MSL_{dt035}), the MSL_p samples have a higher fatigue strength in the whole fatigue regime.

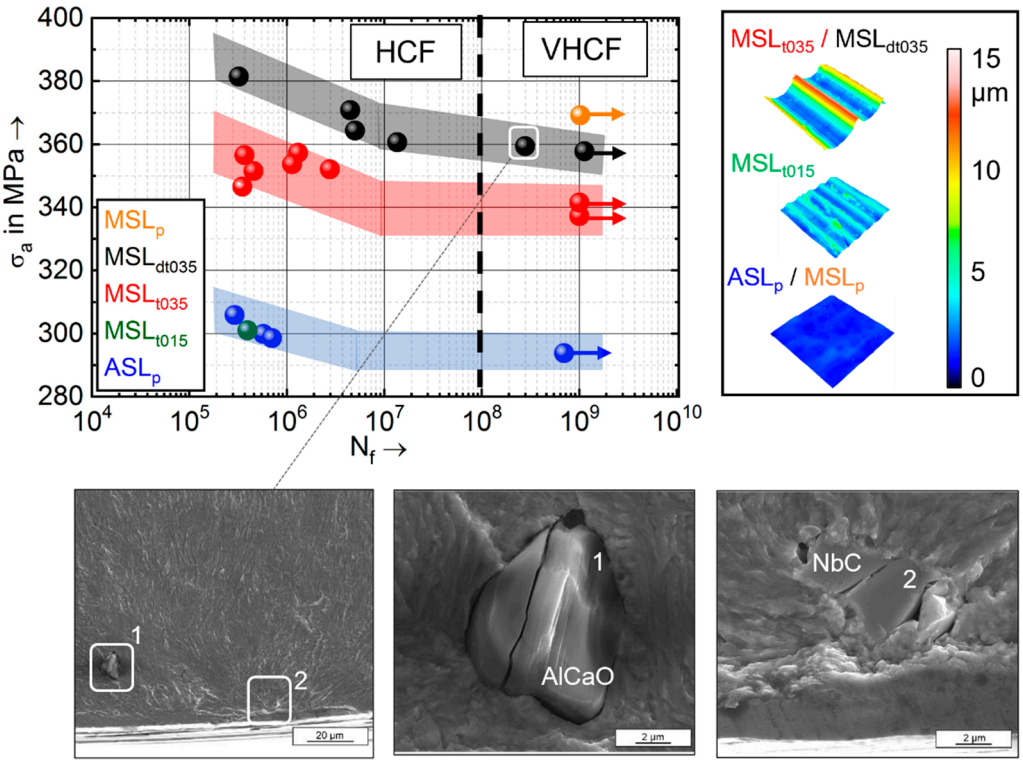

Figure 7. S-N curves of metastable AISI 347 with different surface morphologies and investigation of the surface fracture, run outs are marked with an arrow.

4. Conclusions

The stable austenitic steel AISI 904 and the metastable austenitic steel AISI 347 were investigated with different surface morphologies up to the VHCF regime using an ultrasonic testing system. Microstructural investigations of initial surface morphologies and fracture surface were performed. The study provides the following results:

1. Cryogenic turning of stable AISI 904L (SSL_{t035}) and metastable AISI 347 (MSL_{t035}) results in higher roughness (R_z~11 µm) and tensile residual stresses at the specimen's surface. Moreover, a nanocrystalline layer of a few micrometers under the surface was formed in both materials. In the metastable AISI 347, phase transformation from austenite to martensite was observed additionally. Polishing of the cryogenically turned metastable austenitic specimens (MSL_p) leads to very low average roughness ($R_z < 1$ µm) values and compressive residual stresses at the surface.
2. Fatigue tests of conventionally turned and polished specimens with purely austenitic microstructure in the initial state leads to decreasing S-N curve of stable AISI 904L (SSL_p) in the VHCF regime. With increasing number of cycles to failure, a change from surface to subsurface crack initiation was observed. Opposed to AISI 904L, the AISI 347 (ASL_p) specimens only failed in the HCF regime.
3. Fatigue tests at cryogenic turned specimens show shorter lifetime for specimens of stable AISI 904L (SSL_{t015} and SSL_{t035}) and a lifetime extension for specimen of metastable AISI 347 (MSL_{t035}) even in case of significantly higher surface roughness in comparison to conventionally turned and finally polished samples. The increase in fatigue strength of the cryogenic turned AISI 347 is mainly caused by the machining induced martensitic surface layers.
4. In spite of its smaller monotonic strength, the metastable AISI 347 (MSL_{t035}) reaches a higher HCF and VHCF strength after surface modification by cryogenic turning.
5. The increase of material strength due to pre-deformation and martensitic formation in specimen volume of metastable AISI 347 (MSL_{dt035}) was successful; however, in the VHCF regime a drop in S-N curve was observed.
6. The best fatigue properties are achieved with specimens with surfaces polished after cryogenic turning of metastable AISI 347 (MSL_p).

Author Contributions: Conceptualization, M.S., A.B., D.E., and T.B.; methodology, A.B. and M.S.; experiments and data analysis, A.B. and M.S.; writing original draft, M.S.; review and editing, A.B., D.E., and T.B. All authors have read and agreed to the published version of the manuscript.

Funding: This work was supported by the Deutsche Forschungsgemeinschaft (DFG, German Research Foundation)—project number 172116086—SFB 926 "Microscale Morphology of Component Surfaces".

Institutional Review Board Statement: Not applicable.

Informed Consent Statement: Not applicable.

Data Availability Statement: The data presented in this study are available on request from the corresponding author.

Acknowledgments: The authors thank the German Research Foundation (DFG) for the financial support within the CRC 926 "Microscale Morphology of Component Surfaces". The fatigue specimens were turned at the Institute for Manufacturing Technology and Production Systems (FBK), TU Kaiserslautern, Germany. We thank Aurich J.C. and Kirsch for their support.

Conflicts of Interest: The authors declare no conflict of interest.

References

1. Lai, J.K.L.; Shek, C.H.; Lo, K.H. *Stainless Steels: An Introduction and Their Recent Developments*; Bentham Science Publishers, eBook: United Arab Emirates, 2012; ISBN 1608053059.
2. Smaga, M.; Boemke, A.; Daniel, T.; Klein, M.W. Metastability and fatigue behavior of austenitic stainless steels. *MATEC Web Conf.* **2018**, *165*, 4010. [CrossRef]
3. de Bellefon, G.M.; van Duysen, J.C. Tailoring plasticity of austenitic stainless steels for nuclear applications: Review of mechanisms controlling plasticity of austenitic steels below 400 °C. *J. Nucl. Mater.* **2016**, *475*, 168–191. [CrossRef]
4. Carstensen, J.V.; Mayer, H.; Brønsted, P. Very high cycle regime fatigue of thin walled tubes made from austenitic stainless steel. *Fatigue Fract. Eng. Mater. Struct.* **2002**, *25*, 837–844. [CrossRef]
5. Lago, J.; Jambor, M.; Nový, F.; Bokůvka, O.; Trško, L. Giga-cycle Fatigue of AISI 316L After Sensitising of Structure. *Procedia Eng.* **2017**, *192*, 528–532. [CrossRef]

6. Takahashi, K.; Ogawa, T. Evaluation of Giga-cycle Fatigue Properties of Austenitic Stainless Steels Using Ultrasonic Fatigue Test. *J. Solid Mech. Mater. Eng.* **2008**, *2*, 366–373. [CrossRef]
7. Grigorescu, A.; Hilgendorff, P.-M.; Zimmermann, M.; Fritzen, C.-P.; Christ, H.-J. Fatigue behaviour of austenitic stainless steels in the VHCF regime. In *Fatigue of Materials at Very High Numbers of Loading Cycles: Experimental Techniques, Mechanisms, Modeling and Fatigue Life Assessment*; Christ, H.-J., Ed.; Springer Fachmedien Wiesbaden: Wiesbaden, Germany, 2018; pp. 49–71. ISBN 978-3-658-24531-3.
8. Grigorescu, A.C.; Hilgendorff, P.M.; Zimmermann, M.; Fritzen, C.P.; Christ, H.J. Cyclic deformation behavior of austenitic Cr–Ni-steels in the VHCF regime: Part I—Experimental study. *Int. J. Fatigue* **2016**, *93*, 250–260. [CrossRef]
9. Cherif, A.; Pyoun, Y.; Scholtes, B. Effects of Ultrasonic Nanocrystal Surface Modification (UNSM) on Residual Stress State and Fatigue Strength of AISI 304. *J. Mater. Eng. Perform.* **2010**, *19*, 282–286. [CrossRef]
10. Meyer, D. Cryogenic deep rolling—An energy based approach for enhanced cold surface hardening. *CIRP Ann.—Manuf. Technol.* **2012**, *61*, 543–546. [CrossRef]
11. Aurich, J.C.; Mayer, P.; Kirsch, B.; Eifler, D.; Smaga, M.; Skorupski, R. Characterization of deformation induced surface hardening during cryogenic turning of AISI 347. *CIRP Ann.—Manuf. Technol.* **2014**, *63*, 65–68. [CrossRef]
12. Mayer, P.; Kirsch, B.; Müller, C.; Hotz, H.; Müller, R.; Becker, S.; von Harbou, E.; Skorupski, R.; Boemke, A.; Smaga, M.; et al. Deformation induced hardening when cryogenic turning. *CIRP J. Manuf. Sci. Technol.* **2018**, *23*, 6–19. [CrossRef]
13. Smaga, M.; Skorupski, R.; Eifler, D.; Beck, T. Microstructural characterization of cyclic deformation behavior of metastable austenitic stainless steel AISI 347 with different surface morphology. *J. Mater. Res.* **2017**, *32*, 4452–4460. [CrossRef]
14. Smaga, M.; Skorupski, R.; Mayer, P.; Kirsch, B.; Aurich, J.C.; Raid, I.; Seewig, J.; Man, J.; Eifler, D.; Beck, T. Influence of surface morphology on fatigue behavior of metastable austenitic stainless steel AISI 347 at ambient temperature and 300 °C. *Procedia Struct. Integr.* **2017**, *5*, 989–996. [CrossRef]
15. Boemke, A.; Smaga, M.; Beck, T. Influence of surface morphology on the very high cycle fatigue behavior of metastable and stable austenitic Cr-Ni steels. *MATEC Web Conf.* **2018**, *165*, 20008. [CrossRef]
16. Koster, M. Ultraschallermüdung des Radstahls R7 im Very-High-Cycle-Fatigue (VHCF)-Bereich. Ph.D. Thesis, Technische Universität, Kaiserslautern, Germany, 2011.
17. Man, J.; Smaga, M.; Kuběna, I.; Eifler, D.; Polák, J. Effect of metallurgical variables on the austenite stability in fatigued AISI 304 type steels. *Eng. Fract. Mech.* **2017**, *185*, 139–159. [CrossRef]
18. Eichelmann, G.H.; Hull, T.C. The effect of composition on the temperature of spontaneous transformation of austenite to martensite in 18-8 type stainless steel. *Trans. Am. Soc. Met.* **1953**, *45*, 77–104.
19. Angel, T. Formation of Martensite in Austenitic Stainless Steels—Effects of Deformation, Temperature, and Composition. *J. Iron Steel Inst.* **1954**, *177*, 165–174.
20. Martin, S.; Fabrichnaya, O.; Rafaja, D. Prediction of the local deformation mechanisms in metastable austenitic steels from the local concentration of the main alloying elements. *Mater. Lett.* **2015**, *159*, 484–488. [CrossRef]
21. Smaga, M.; Boemke, A.; Daniel, T.; Skorupski, R.; Sorich, A.; Beck, T. Fatigue Behavior of Metastable Austenitic Stainless Steels in LCF, HCF and VHCF Regimes at Ambient and Elevated Temperatures. *Metals* **2019**, *9*, 704. [CrossRef]
22. Daniel, T.; Smaga, M.; Beck, T. Cyclic deformation behavior of metastable austenitic stainless steel AISI 347 in the VHCF regime at ambient temperature and 300 °C. *Int. J. Fatigue* **2022**, *156*, 106632. [CrossRef]
23. Hornbach, D.J.; Prevéy, P.S.; Mason, P.W. X-ray diffraction charcterization of the residual stress and hardness distributions in induction hardened gears. In Proceedings of the First International Conference on Induction Hardened Gears and Critical Components, Indianapolis, IN, USA, 15–17 May 1995; pp. 69–76.
24. Talonen, J.; Aspegren, P.; Hanninen, H. Comparison of different methods for measuring strain induced alpha-martensite content in austenitic steels. *Mater. Sci. Technol.* **2004**, *20*, 1506–1512. [CrossRef]
25. M'Saoubi, R.; Outeiro, J.C.; Changeux, B.; Lebrun, J.L.; Morão Dias, A. Residual stress analysis in orthogonal machining of standard and resulfurized AISI 316L steels. *J. Mater. Process. Technol.* **1999**, *96*, 225–233. [CrossRef]
26. Chai, G.; Zhou, N. Study of crack initiation or damage in very high cycle fatigue using ultrasonic fatigue test and microstructure analysis. *Ultrasonics* **2013**, *53*, 1406–1411. [CrossRef] [PubMed]
27. Schwerdt, D.; Pyttel, B.; Berger, C. Fatigue strength and failure mechanisms of wrought aluminium alloys in the VHCF-region considering material and component relevant influencing factors. *Int. J. Fatigue* **2011**, *33*, 33–41. [CrossRef]
28. Khan, M.K.; Wang, Q.Y. Investigation of crack initiation and propagation behavior of AISI 310 stainless steel up to very high cycle fatigue. *Int. J. Fatigue* **2013**, *54*, 38–46. [CrossRef]
29. Müller-Bollenhagen, C.; Zimmermann, M.; Christ, H.J. Very high cycle fatigue behaviour of austenitic stainless steel and the effect of strain-induced martensite. *Int. J. Fatigue* **2010**, *32*, 936–942. [CrossRef]
30. Müller-Bollenhagen, C.; Zimmermann, M.; Christ, H.J. Adjusting the very high cycle fatigue properties of a metastable austenitic stainless steel by means of the martensite content. *Procedia Eng.* **2010**, *2*, 1663–1672. [CrossRef]